

TLB 型复杂焊接结构超声 SH 导波成像检测

朱新杰, 韩赞东, 都 东, 陈以方*

(清华大学先进成形制造教育部重点实验室, 北京 100084)

摘 要: 通过光弹试验分析超声水平剪切(shear horizontal, SH)导波具有优异传播性能, 构建了超声导波成像检测系统, 基于合成孔径聚焦对超声 SH 导波用于 TLB 型式复杂焊接结构成像检测进行了重点研究. 结果表明, 基于合成孔径聚焦的超声 SH 导波成像用于 TLB 型式复杂焊接结构构件检测是可行的, 检测图像能够表征板材中区域特征, 对焊缝有较好的定位功能, 但在焊缝之后会形成长约 100 mm 的固有散射盲区. 文中为进一步提高 TLB 型式复杂焊接结构超声导波成像检测应用水平提供了基础.

关键词: 超声 SH 导波; 复杂焊接结构; 成像检测

中图分类号: TB553 文献标识码: A 文章编号: 0253-360X(2012)09-0029-04



朱新杰

0 序 言

大尺度复杂焊接结构板材在大型反应器、造船、油气管道、石油储备等领域应用广泛. 超声板中导波检测是实现这类焊接结构板材无损检测的重要方法之一, 其中水平剪切(shear horizontal, SH)导波在这类大尺度钢板焊接结构成像检测、结构健康检测中具有重要的应用价值. 单一金属板中的超声 SH 导波、Lamb 波在传播中存在着声场变化、声波与孔、槽等人工散射体的相互作用^[1-5], 这些情况在有焊接结构的条件下会更加复杂, 将严重削弱成像检测数组信号的双曲线特征, 进而影响成像质量. 这使得在对焊接结构板材进行超声导波成像检测中, 必须合理选用导波类型、模态、成像原理及成像算法、换能器种类. 板中超声导波成像检测研究中换能器数组有线型数组^[6]、环型数组^[7]、稀疏型数组^[8]等不同的布置形式, 这些成像检测对象大多是单一金属板材, 很少涉及焊接结构板材.

T 形焊缝、搭接焊缝(lap joint)、对接焊缝(butt joint)等同时构成了一类重要的具有空间位置关系、复杂的 TLB 型焊接结构. 文中基于合成孔径聚焦, 将换能器布置成线型数组, 对超声导波用于 TLB 型复杂焊接结构构件成像检测进行了重点研究, 将为进一步研究并提高大尺度复杂焊接结构板材超声导波成像检测与应用水平提供基础.

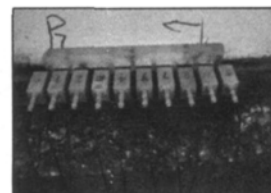
1 TLB 型复杂焊接结构及其超声导波成像检测系统构成

1.1 TLB 型式复杂焊接结构

检测工程中会遇到大尺度焊接结构, 在油气储罐的立板、底板等焊接结构中, 如图 1, 图 2 所示, 立板是钢板之间的对接焊接, 立板与底板之间是 T 形焊接, 底板是钢板之间的搭接焊接, 即整个焊接结构中焊缝 I 是 T 形焊缝, 焊缝 II 和焊缝 III 是搭接焊缝, 焊缝 IV 是对接焊缝, 这 3 种焊接结构构成了 TLB 型复杂焊接结构. TLB 型式复杂焊接结构为一类典型的工业在役焊接结构, 钢板材料为 Q235A, 底板厚为 8 mm, 立板厚为 14 mm.



(a) 油气储罐



(b) 油气储罐超声成像检测

图 1 油气储罐超声导波成像检测现场

Fig. 1 Imaging and testing of ultrasonic guided wave for oil and gas tank in-site

1.2 超声导波类型的选择

为了选择适用于 TLB 型复杂焊接结构超声导波成像检测的导波类型, 进行了板中光弹试验研究.

收稿日期: 2011-06-27

基金项目: 国家自然科学基金资助项目(60871101)

* 参加此项研究工作的还有原可义

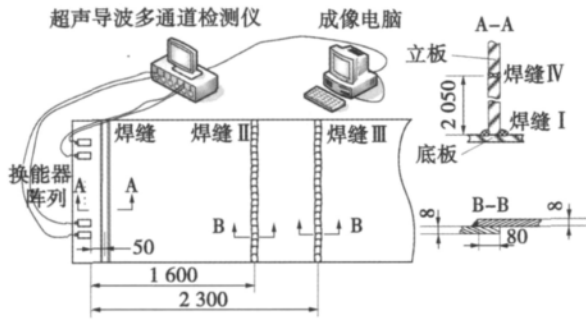


图 2 TLB 型式焊接结构及其超声导波成像检测系统构成 (mm)

Fig. 2 TLB weld structure and its imaging and testing system

板中光弹试验显示如图 3 所示,在板中传播时 SH 导波由于结构简单,能量集中在波头,经过几次端面反射后,波型转换较少,波列和波头较紧凑,这使得检测距离较大时检测分辨率较高,检测盲区较小,有利于进行声波信号分析和成像; Lamb 波在传播中,由于模态复杂,单一模态不易激发,往往是 2 种以上模态混杂,波列松散且展宽较大,波头虽然明显,但能量是分布在较宽的波列中,当经过头反射后由于波型转换严重,这使得检测距离较大时分辨率较低,检测盲区较大,不利于进行声波信号分析和成像. 另外 SH 导波传播只决定于板材面内质点位移,板材表面有无液体、污物等对其传播影响不大,表面能量泄露较少.

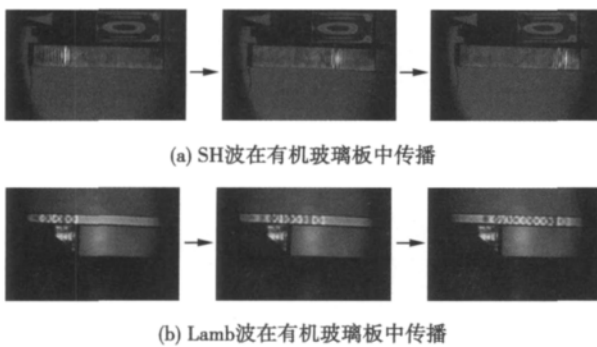


图 3 有机玻璃板中 SH 波与 Lamb 波光弹试验

Fig. 3 Photoelastic experiment of ultrasonic guided waves in plexiglass plate

由图 3 可见,同等检测条件下,超声 SH 导波有较好的模态可控性、波形持续性和较小的表面能量泄露. 工业在役焊接结构板材超声导波成像检测,选用产生 SH 导波的压电楔形换能器有较高的能量转换效率,将多个 SH 导波换能器布置成数组对板

材进行成像检测,将能有效发挥 SH 导波的检测优势. 因此对于 TLB 型焊接结构构件超声导波成像检测,文中优先选择超声 SH 导波.

1.3 超声导波成像系统构成

根据压电效应研制了 SH 导波换能器(阵元),将其与自行研制的多信道导波检测仪、TLB 型焊接结构构件组成了如图 2 所示的现场成像检测试验系统. 在 TLB 焊接结构构件底板边缘处布置有 10 个 SH 导波换能器构成线型数组,换能器(阵元)主频为 1 MHz,数组布阵间距为 5 mm,方波脉冲激发换能器在钢板中产生的超声 SH 导波模态以 0 阶模态为主,人工缺陷回波信号主频在 0.45 MHz 左右,通过测定可选择最佳脉冲激励频率为 0.5 MHz.

2 超声 SH 导波成像原理

合成孔径聚焦可被用于 TOFD 的检测中^[9,10]. 文中基于合成孔径聚焦利用超声 SH 导波对板材中超声散射体进行成像,现将原理做简要讨论.

在给定的坐标系中布置 n 个 SH 导波换能器组成的线型数组,设发射阵元坐标为 (x_0, y_0) ,第 i 个阵元发射信号被成像区域内任意散射体 $P(x, y)$ 反射后被第 i 个阵元接收时的渡越时间为 t_i ,且第 i 个阵元发射信号被成像区域内任意散射体 $P(x, y)$ 反射后被第 j 个阵元接收时的渡越时间为 t_j ,引入比例因子 k_0, k_{ij} 分别反映反射信号(能量) S_{ij} 、反射合成信号(能量) $S(t, r, \theta)$ 与反射信号回波幅度 $U_{ij}^2(x, y)$ 、反射信号总回波幅度 $U^2(x, y)$ 的正比关系,那么阵元依次发射、所有阵元分别接收到散射体 $P(x, y)$ 反射的合成信号能量为

$$S(x, y) = \sum_{i=1}^n \sum_{j=1}^n S_{ij}(t_i - t_j) \quad (1)$$

通过式(1)得到对散射体 $P(x, y)$ 信号聚焦后总信号回波幅值(能量)为

$$U(x, y) = \sqrt{\frac{1}{k_0} \cdot \sum_{i=1}^n \sum_{j=1}^n k_{ij} \cdot U_{ij}^2(t_i - t_j)} \quad (2)$$

这样,对得到的 n 组信号进行“移相合成”的时空域信息处理,就可完成对点 $P(x, y)$ 的“全场域聚焦”.

SH 导波群速度 v_g 是频率 ω 的函数,与 SH 导波模态有关,式(2)中的渡越时间 t_i 为

$$t_i = t'_i + \Delta t_i = 2 \sqrt{(x - x_0)^2 + (y - y_0)^2} / v_g + 2l_i / \bar{v} \quad (i = 1, 2, \dots, n) \quad (3)$$

式中: l_i 为第 i 个阵元结构参数,为从阵元内压晶体管到阵元前沿的当量声程; \bar{v} 为换能器楔块内的平

均声波速度; t'_i 为声波在换能器以外的渡越时间; Δt_i 为声波在换能器内部的渡越时间.

设待检测材料衰减系数为 α , 考虑补偿声波在声程 r 处的衰减, 则散射体 $P(x, y)$ 在 256 级图像中的像素灰度为

$$f(x, y) = 256 \times \frac{U(x, y) e^{\alpha r} - U_{\min}}{U_{\max} - U_{\min}} \quad (4)$$

式中: U_{\max}, U_{\min} 分别为 $U(x, y)$ 的最大值和最小值. 将式(2)代入式(4)就得到成像区域内任意散射体 $P(x, y)$ 的图像, 即所成图像灰度值为

$$f(x, y) = 256 \times \frac{e^{\alpha r} \sqrt{\frac{1}{k_0} \sum_{i=1}^n \sum_{j=1}^n k_{ij} \cdot U_{ij}^2(t_i - t_j)} - U_{\min}}{U_{\max} - U_{\min}} \quad (5)$$

3 TLB 型复杂焊接结构成像检测试验

3.1 TLB 型复杂焊接结构成像检测数组信号

对 TLB 型焊接结构进行现场在役成像检测试验, 检测距离 d 为 4 m 声程范围内的数组信号较明显, 4 道焊缝的数组信号概貌清晰可见. 2.4 m 内信号的数组特征较强, 2.4 ~ 4 m 之间信号的数组双曲线特征稍弱, 是由声波在多个散射体处的散射、不可避免的波形转换、声波传播路径的变化所至, 如图 4 所示.

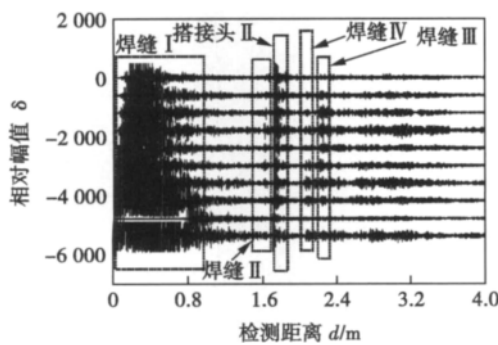


图 4 成像检测数组波形

Fig. 4 Array signals of imaging and testing

焊缝 I 为 T 形焊缝, 从信号数组特征上看, 该信号的声程扩展达到了近 1 m, 这是由于“自发自收”的换能器发射声波时首先在 T 形焊缝和底板外边缘端部来回反射所至. 由于长期暴露在空气中, 底板外边缘的表面形成了直径为 1 ~ 2 mm 的不规则蚀坑, 导致换能器与底板之间的耦合面极不平整, 耦合层较厚, 造成声波信号有近 30 dB 的衰减, 为了使声波传播尽可能远, 声波的发射增益较大, 达到了近

40 dB, 所以 T 形焊缝与底板外边缘端面之间的来回声波反射较强烈.

焊缝 II 是搭接焊缝, 位于检测距离 d 为 1.6 m 处, 如图 5 所示, 其搭接头 II 的反射信号在焊缝 II 的信号之后到达, 二者声程差约为 80 ~ 120 mm, 搭接头的信号幅值远大于焊缝, 符合实际情况. 焊缝及搭接头有较大的线性尺度, 声波散射严重, 典型的双曲线数组特征不明显.

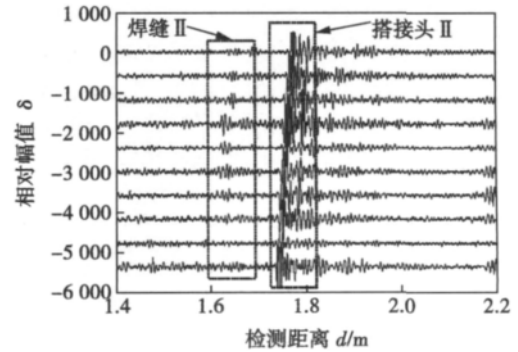


图 5 焊缝 II 的数组信号

Fig. 5 Array signals of weld II and lap II

焊缝 III 也是搭接焊缝, 处于检测距离 d 约为 2.3 m 处, 由于声程的改变和焊缝散射, 焊缝 III 与其搭接头信号不能区分. 在焊缝 III 之前是 d 为 2.1 m 处的立板中的第 4 道对接焊缝 IV, 从声程上看焊缝 III 和焊缝 IV 相距约为 200 mm, 这两道焊缝分别位于 TLB 型焊接结构构件立体空间中的不同部位, 虽然信号幅值都较弱, 但依然能分辨, 如图 6 所示.

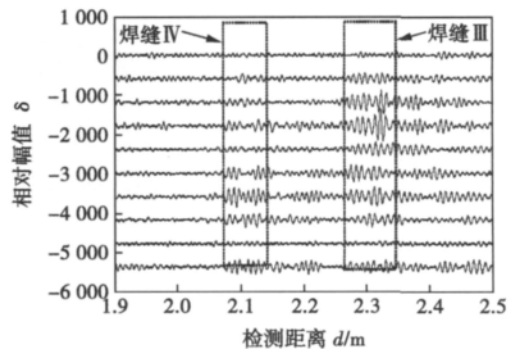


图 6 焊缝 III 和焊缝 IV 的数组信号

Fig. 6 Array signals of weld III and weld IV

3.2 TLB 型焊接结构超声导波成像检测图像

对 TLB 型焊接钢板构件用超声 SH 导波进行现场成像检测试验, 成像结果如图 7 所示, 考虑到成像检测要实现较大的有效检测距离, 根据现场情况和成像检测换能器阵元数量, 成像检测距离 d 取 1.5

~3.5 m, 成像宽度 w 为 450 mm. 结合该检测图像在第 105 行的灰度曲线进行分析, 1.6 m 处为焊缝 II, 约 1.7 m 处为焊缝 II 的搭接头 II, 2.1 m 处为焊缝 IV, 在 2.3 m 处为焊缝 III, 在 2.7 m 处、3.1 m 等处也有较微弱的图像显示, 如图 8 所示.

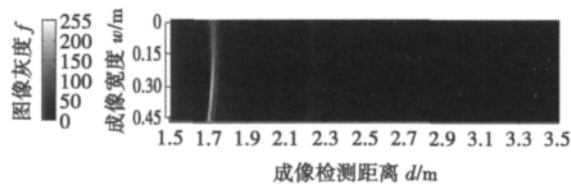


图7 TLB 型式复杂焊接结构成像检测图像

Fig.7 Image of imaging and testing for TLB weld structure in service

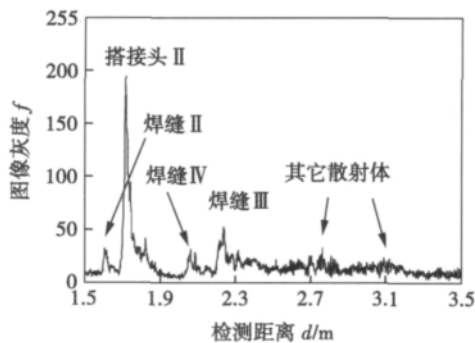


图8 TLB 型式复杂焊接结构成像检测图像灰度曲线

Fig.8 Scale curve of image of imaging and testing for TLB weld structure in service

焊缝 II 与其搭接头 II 虽然能在图像中较好地地区分, 但在 1.7 m 处的搭接头 II 之后却形成了强烈的散射区, 如图 7 所示, 该区域内尺寸当量较小的缺陷散射体有可能被漏检, 形成焊缝散射盲区, 长度约为 100 mm 左右, 该盲区与声波散射特性相关, 是固有的、不可调节的, 在实际检测中该盲区内的漏检、误检问题要予以重点关注.

文中成像系统在实验室条件下可对超过 3 m 检测距离远处 $\phi 10$ mm 尺寸当量的孔缺陷进行超声导波图像表征, SH 导波在 TLB 型式焊接结构中传播具备较远距离的可达性, 可认为图 7 和图 8 所示的现场成像检测图像中不存在大于 $\phi 10$ mm 孔当量尺寸的缺陷, 现场其它检测方法也证实了这一点.

用超声 SH 导波对 TLB 型式复杂焊接结构板材进行成像检测, 搭接焊缝及其搭接端头成像细节较清楚, 可实现对焊缝的准确定位. 但该方法对 TLB 型大尺度复杂焊接结构构件中的较小腐蚀缺陷、焊缝中缺陷的成像检测、不同性质缺陷的空间位置判(识)

别等仍需要进一步研究, 这在导波成像检测中仍将是挑战性较强的课题.

4 结 论

(1) 超声 SH 导波比 Lamb 波有更好的模态可控性、较好的波形连续性、小的表面能量泄露, 基于此将研制的 SH 导波压电楔形换能器可布置成线形数组对 TLB 型复杂焊接结构进行成像检测, 有效发挥了 SH 导波的检测长处.

(2) 基于合成孔径的超声 SH 导波成像方法可用于 TLB 型复杂焊接结构构件的成像检测, 所成图像能够表征构件中的焊缝结构等区域特征, 对检测区域特征有较好的定位功能.

(3) 由于焊缝对声波形成散射, 导波成像时在搭接焊缝后形成了约为 100 mm 长的焊缝散射盲区, 在进一步研究与实际检测中对该盲区中的漏检、误检问题要予以重点关注.

参考文献:

- [1] Zhao Xiaoliang, Joseph L R, Sam Pelts. Quantitative NDE potential in a waveguide with lamb and shear horizontal waves[J]. American Institute of Physics Conference Proceedings, 2002, 615 (5): 196-202.
- [2] Predoi M V. Wave propagation along transversely periodic structures[J]. The Journal of the Acoustical Society of America, 2007, 121(4): 1935-1944.
- [3] Castaings M, Lowe M. Finite element model for waves guided along solid systems of arbitrary section coupled to infinite solid media[J]. The Journal of the Acoustical Society of America, 2008, 123(2): 696-708.
- [4] Ratassep M, Loweb M J S, Cawley P, et al. Scattering of the fundamental shear horizontal mode in a plate when incident at a through crack aligned in the propagation direction of the mode[J]. The Journal of the Acoustical Society of America, 2008, 124(5): 2873-2882.
- [5] Ma J, Cawley P. Low-frequency pulse echo reflection of the fundamental shear horizontal mode from part-thickness elliptical defects in plates[J]. The Journal of the Acoustical Society of America, 2010, 127(6): 3485-3493.
- [6] Lingyu Y, Giola B S, Victor G. Shear lag solution for tuning ultrasonic piezoelectric wafer active sensors with applications to Lamb wave array imaging[J]. International Journal of Engineering Science, 2010, 48(10): 848-861.
- [7] Velichko A, Wilcox P D. Guided wave arrays for high resolution inspection[J]. The Journal of the Acoustical Society of America, 2008, 123(1): 186-196.

Lei Zhen , Lin Shangyang , Wang Xuyou. A welding technology of laser-digital controlled short circuiting transfer arc hybrid welding: A new high-efficient welding technology replaced TIG welding with filler wire [J]. *Welding & Joining* , 2009(5) : 23 - 26.

- [4] 刘西洋, 孙凤莲, 王旭友. Nd: YAG 激光 + CMT 电弧复合热源横焊工艺参数对焊缝形貌的影响 [J]. *焊接学报* , 2010 , 31 (9) : 109 - 112.

Liu Xiyang , Sun Fenglian , Wang Xuyou. Influences of Nd: YAG laser + CMT arc hybrid horizontal welding parameters on the weld

morphology [J]. *Transactions of the China Welding Institution* , 2010 , 31(9) : 109 - 112.

作者简介: 刘西洋, 男, 1980 年出生, 硕士研究生. 主要研究方向为激光 + MIG 电弧复合热源焊接技术. 发表论文 3 篇. Email: 2004liuxiyang@163.com

通讯作者: 王旭友, 男, 硕士, 研究员, 硕士研究生导师. Email: wangxuyou@tom.com

[上接第 32 页]

- [8] Michaels J E , Hall J S , Michaels T E. Adaptive imaging of damage from changes in guided wave signals recorded from spatially distributed arrays [J]. *Proceedings of International Society for Optical Engineering* , 2009 , 7295(15) : 1 - 11.

- [9] 刚 铁, 迟大钊, 袁 媛, 基于合成孔径聚焦的超声 TOFD 检测技术及图像增强 [J]. *焊接学报* , 2006 , 27(10) : 7 - 10. Gang Tie , Chi Dazhao , Yuan Yuan. Ultrasonic TOFD technique and image enhancement based on synthetic aperture focusing technique [J]. *Transactions of The China Welding Institution* , 2006 , 27(10) : 7 - 10.

- [10] 迟大钊, 刚 铁, 姚英学, 等. 一种基于超声 TOFD 法的近表面缺陷检测模式 [J]. *焊接学报* , 2011 , 32(2) : 25 - 28.

Chi Dazhao , Gang Tie , Yao Yingxue , *et al.* Mode for near surface defect detection based on ultrasonic TOFD [J]. *Transactions of the China Welding Institution* , 2011 , 32(2) : 25 - 28.

作者简介: 朱新杰, 男, 1977 年出生, 博士研究生. 主要研究方向为超声无损检测和评估. 发表论文 7 篇. Email: zxjconcrete@163.com.

通讯作者: 都 东, 男, 1962 年出生, 博士, 教授, 博士研究生导师. Email: dudong@tsinghua.edu.cn

Numerical analysis of TIG welding pool at step parameter

HUANG Jiankang² , GUO Chaobo² , SHI Yu¹ , FAN Ding¹ (1. State Key Laboratory of Gansu Advanced Non-ferrous Metal Materials , Lanzhou University of Technology , Lanzhou 730050 , China; 2. Key Laboratory of Non-ferrous Metal Alloys and Processing , The Ministry of Education , Lanzhou University of Technology , Lanzhou 730050 , China) . pp 17 – 20 , 28

Abstract: A three-dimensional model of freely burning TIG arc was developed. By using FLUENT software , choosing appropriate boundary conditions and strongly coupling control equations , TIG welding pool was simulated. Under the action of different parameters , the changing of size and temperature of the pool were analyzed. The results show that with the high current stepping to the low current , the pool size and the flow will decrease at some extent. With the step of the welding voltage , welding speed , workpiece thickness and width , the changes show a certain lag. By adjusting the welding parameters , the pool size can be controlled.

Key words: TIG welding; pool; numerical analysis; FLUENT

Ultrasonic friction stir welding of LF21 aluminum alloy

MA Huikun , HE Diqiu , LIU Jinshu (College of Mechanical and Electrical Engineering of Central South University , Changsha 430081 , China) . pp 21 – 23

Abstract: According to the principle of the role of ultrasound on metal plastic forming , the self-developed ultrasonic friction stir welding machine was used to weld LF21 aluminum alloy plates. The microstructures and fracture appearance of aluminum alloys were studied. Experiments show that the ultrasonic energy can inject into the weld joint effectively. It can not only increase the intensity of the bottom of weld joint , but also improve metal atoms motion and diffusion ability around mixing needle. The grain in microstructure of WNZ (weld nugget zone) is refined and homogenized obviously. The tensile fracture of ultrasonic friction stir welded joint appears to be a dimple pattern. The depth of dimple is shallower and the number of dimples is less than that in the fracture of friction stir welding. The result shows that ultrasonic welding can improve the mechanical properties of the joint , but the elongation decreases a little compared to that of friction stir welding.

Key words: friction stir welding; ultrasonic; LF21

Determination of material parameters for welding process simulation

YAN Dejun¹ , LIU Xuesong² , YANG Jianguo² , FANG Hongyuan² , YANG Yongqiang¹ (1. Guangdong General Research Institute for Industrial Technology , Institute of Welding Technology , Guangzhou 510650 , China; 2. State Key Laboratory of Advanced Welding and Joining , Harbin Institute of Technology , Harbin 150001 , China) . pp 24 – 28

Abstract: Thermo-mechanical parameters varied with temperature were used to compare qualitatively the influence of the yield strength , heat conductivity , specific heat capacity , Young's modulus , coefficient of thermal expansion , density and Poisson ratio on the peak welding residual stress. The result shows that the change of yield strength and heat conductivity is wide , which have greater effects on the peak welding residual

stress. Whereas , specific heat capacity , Young's modulus , coefficient of thermal expansion and density show little influence on it. The change of Poisson ratio is close to that of thermal expansion and density , however , its influence is little. The simulation results of welding longitudinal residual stress were verified with cutting pieces stress relieving method for the flat plates with such material properties as 2A12-T4 aluminum alloy. The results have good agreement with tested results , which prove the validity of the simulation results.

Key words: numerical simulation; longitudinal residual stress; material parameters; stress peak value

Ultrasonic SH guided waves imaging and test on complicated TLB welded structure

ZHU Xinjie , HAN Zandong , DU Dong , CHEN Yifang (Key Laboratory for Advanced Materials Processing Technology , the Ministry of Education , Tsinghua University , Beijing 100084 , China) . pp 29 – 32 , 48

Abstract: The T-joint welding , the lap welding and the butt welding constitute an important and complicated industrial structure named TLB type welded structure , where imaging and testing of ultrasonic guided waves has an important influence. The testing and imaging experiment system of ultrasonic SH-guided wave for TLB type welded structure was developed. It can be known from the dynamic photoelastic experiments that ultrasonic SH (shear horizontal) guided waves technology is more suitable for testing and imaging TLB type welded structure. The imaging principle of ultrasonic guided waves in plate was discussed , and the imaging and testing of SH guided waves in TLB type welded structure was researched. The experiment results shows that it is possible for SH guided waves to image and test TLB type welded structure , which may characterize the welded structure in the testing area , and its image has the positioning function for the testing regional features. Nevertheless , in imaging there may be a weld scattering blind area , about 100 mm behind the weld , which is the inherent ultrasonic scattering properties of the weld. The topic proposed provides the basis for further researching and improving imaging and testing of SH guided waves in complicated TLB type welded structure.

Key words: ultrasonic SH guided waves; complicated welded structure; imaging and testing

Research on interfacial fracture behavior of TBCs/Q345 based on local approach

YANG Zhen^{1,2} , JING Hongy-ang^{1,2} , XU Lianyong^{1,2} (1. School of Materials Science and Engineering , Tianjin University , Tianjin 300072 , China; 2. Tianjin Key Laboratory of Advanced Joining Technology , Tianjin 300072 , China) . pp 33 – 36

Abstract: The critical load at crack propagation for the coated specimens was obtained through the tensile test , and the finite element method (FEM) was conducted to simulate the fracture behavior by ABAQUS code. Then the results from FEM were input into a self-programmed FORTRAN code , the two parameters of Weibull distribution dominating the interfacial fracture were obtained. The mathematical formula of the local approach applied to analyze the interface fracture was deduced. After that , the local approach was adopted to analyze the crack-size dependence of coating specimens for interface brittle fracture ini-